JCTC Journal of Chemical Theory and Computation

The IMOMM (Integrated Molecular Orbitals/Molecular Mechanics) Approach for Ligand-Stabilized Metal Clusters. Comparison to Full Density Functional Calculations for the Model Thiolate Cluster $Cu_{13}(SCH_2CH_3)_8$

Alexander Genest,[†] André Woiterski,[†] Sven Krüger,[†] Aleksey M. Shor,[‡] and Notker Rösch*,[†]

Department Chemie, Theoretische Chemie, Technische Universität München, 85747 Garching, Germany, and Institute of Chemistry and Chemical Technology, Russian Academy of Sciences, 660049 Krasnoyarsk, Russian Federation

Received August 12, 2005

Abstract: To validate the IMOMM (integrated molecular orbitals/molecular mechanics) method for ligand-stabilized transition metal clusters, we compare results of this combined quantum mechanical and molecular mechanical (QM/MM) approach, as implemented in the program ParaGauss (Kerdcharoen, T.; Birkenheuer, U.; Krüger, S.; Woiterski, A.; Rösch, N. *Theor. Chem. Acc.* **2003**, *109*, 285), to a full density functional (DF) treatment. For this purpose, we have chosen a model copper ethylthiolate cluster, $Cu_{13}(SCH_2CH_3)_8$ in D_{4h} symmetry. The evaluation is based on 16 conformers of the cluster which exhibit single and bridging coordination of the ligands at the Cu_{13} cluster as well as various ligand orientations. For corresponding isomers, we obtained moderate deviations between QM and QM/MM results: 0.01−0.06 Å for pertinent bond lengths and up to ∼15° for bond angles. Ligand binding energies of the two approaches deviated less than 6 kcal/mol. The largest discrepancies between full DF and IMOMM results were found for isomers exhibiting short Cu−H and H−H contacts. We traced this back to the localization of different minima, reflecting the unequal performance of the DF and the force-field methods for nonbonding interactions. Thus, QM/MM results can be considered as more reliable because of the well-known limitations of standard exchange-correlation functionals for the description of nonbonding interactions for this class of systems.

Introduction

Accurate quantum chemical methods are restricted to calculations on small to mid-size systems. Large molecular species, like complexes with bulky ligands occurring in homogeneous catalysis or biomolecules, still have to be treated either by a less accurate approach or by a combination of quantum mechanical and molecular mechanical methods (QM/MM).[1−3] Combined approaches such as the integrated molecular orbitals/molecular mechanics (IMOMM) method,[4] a QM/MM variant, have found widespread use for treating systems where only a small part has to be described with high accuracy and the remaining part of the system can be considered as an "environment", exerting steric constraints or acting as a support. Typical examples of such systems are homogeneous catalysts with bulky ligands,[5,6] metal centers of heterogeneous catalysts at oxide surfaces or in zeolites cavities,[7] self-assembled monolayers at gold surfaces,[8] solvated complexes,[9−11] and large molecules of biological interest.[12−14]

Ligand-stabilized transition metal clusters can be viewed in analogy to metal complexes. The metal core features a

* Corresponding author tel. +49 89 289 13620; e-mail: roesch@ch.tum.de.

[†] Technische Universität München.

[‡] Russian Academy of Sciences.

10.1021/ct050202r CCC: $33.50
Published on Web 11/30/2005

rather complex electronic structure which, at least for metal centers in direct contact with ligands, easily responds to ligand binding. Thus, the electronic structure of the subsystem, which comprises the metal cluster proper and the metal−ligand bonds, has to be treated at a sophisticated level. In contrast, interligand interactions most often are dominated by van der Waals or electrostatic forces, which are amenable to modeling by a force-field approach.

Extending our previous work on small model complexes,[15] we apply here a recently developed implementation of the IMOMM approach to ligand-stabilized transition metal clusters. To the best of our knowledge, this is the first application of a QM/MM method to metal cluster compounds. To assess the accuracy of the IMOMM approach, we compare its results to those of the corresponding all-electron treatment. For this purpose, we have chosen the copper thiolate cluster $Cu_{13}(SCH_2CH_3)_8$ as a simple yet realistic example. In this way, we will validate our implementation and examine the performance of the IMOMM approach for a new class of systems. The choice of our model compound has been inspired by gold thiolate clusters, which recently attracted considerable interest as versatile building blocks of nanostructured materials and as realizations of quantum dots.[16,17] Although most of the experimental work on transition metal thiolate clusters is devoted to gold species, the corresponding copper compounds have also been synthesized.[18,19] The special interest in thiolate-stablized metal clusters is due to their rather simple synthesis, yielding stable products that are easy to handle, as well as the versatile chemistry of the thiolate ligands, which allows tailoring of the cluster surface for various purposes.[20,21]

This work is organized as follows. We briefly review the IMOMM method, proceed to describe specific features of the IMOMM implementation of the parallel density functional (DF) program ParaGauss,[22,23] and discuss other computational details. Then, we present the model cluster $Cu_{13}(SCH_2CH_3)_8$ and discuss its properties on the basis of DF calculations. Subsequently, we compare these results to those of IMOMM calculations which combine DF and force-field methods.

The IMOMM Implementation of ParaGauss

The QM/MM approach used in the present work is an adaptation of the IMOMM method,[4] which, besides standard IMOMM calculations, also allows one to treat ligated metal clusters.[15] In a QM/MM approach, one starts with partitioning a complex system *XY* into a "central" part *X*, treated by an accurate QM method, and its "environment" *Y*, described in an approximate way at a MM level. Correspondingly, one separates the total energy as

$$E(XY) = E_{QM}(X) + E_{MM}(Y) + E_{INT}(X,Y) \quad (1)$$

In the IMOMM method,[4] one approximates the interaction energy $E_{INT}(X,Y)$ between the two subsystems by its value at the lower level of accuracy (MM)

$$E_{INT}(X,Y) \approx E_{INT}^{appr}(X,Y) = E_{MM}(XY) - E_{MM}(X) - E_{MM}(Y) \quad (2)$$

This results in an "extrapolation" or "difference" scheme:[3,4]

$$E(XY) \approx E_{appr}(XY) = E_{QM}(X) + E_{MM}(XY) - E_{MM}(X) \quad (3)$$

For ligand-stabilized metal clusters, one has to cut covalent bonds (frontier bonds) of the ligands when one partitions the system *XY*. It is customary to cap the resulting "dangling" bonds of the QM region by "link atoms".[24] Different from the original approach,[4] the IMOMM implementation of ParaGauss[15] constrains the location $\vec{R}_2$ of link atoms to lie in the direction of the corresponding frontier bond from an atom at $\vec{R}_1$ (QM side) to an atom at $\vec{R}_3$ (MM side), by applying a fixed scaling factor *g*:[25]

$$\vec{R}_2 = \vec{R}_1 + g(\vec{R}_3 - \vec{R}_1) \quad (4)$$

Alternatively, one may keep these link bonds at a fixed length. Both procedures yield very similar results if the various parameters are suitably chosen.[15]

The IMOMM variant just described has been implemented in the parallel DF program package ParaGauss.[22,23] The implementation relies on the newly developed MM module MOLMECH[26] of ParaGauss and the geometry-optimizing module OPTIMIZER.[27] This new module of ParaGauss simplifies QM/MM calculations compared to the previous implementation,[15] which invoked an external MM program. QM/MM calculations carried out with MOLMECH benefit from the efficient symmetry treatment of ParaGauss.[28] The capability for QM/MM calculations is implemented in ParaGauss as an interface module which exchanges data between QM and MM modules on one hand and the OPTIMIZER module on the other. Relevant tasks are the preparation and distribution of data derived from a master input, the gathering of QM and MM contributions to energy gradients, and finally the calculation of the total QM/MM energy of the entire system *XY*.[15]

The module MOLMECH was designed to perform energy minimizations of molecules as well as of systems with two- and three-dimensional periodic boundary conditions for which atomic positions as well as unit cell parameters can be optimized. MOLMECH features a general open structure of force-field terms, which allows easy extension by new terms or new parameter sets. Electrostatic interactions of isolated molecules are treated either by a direct sum over atomic charges or by bond-centered dipoles as realized in the MM3 force field.[29] Electrostatic and van der Waals interactions of isolated systems are evaluated without cutoffs. Long-range electrostatic interactions in periodic systems, for example, in two- or three-dimensional arrays of ligated metal clusters, are calculated by Ewald techniques.[30,31] As this treatment of electrostatics is the computationally most-demanding part of a force field (FF) calculation, it has been parallelized employing the communication interface of ParaGauss.[22,23]

Computational Details

All QM calculations were carried out with the linear combination of Gaussian-type orbitals fitting-functions DF method[32] (LCGTO-FF-DF) as implemented in the parallel quantum chemistry package ParaGauss.[22,23] The geometry of the various systems was optimized using the local density

approximation (LDA)[33] for the exchange-correlation potential. LDA is well-known to yield reliable equilibrium geometries for transition metal compounds.[34−36] In contrast, LDA functionals tend to overestimate binding energies.[34] Therefore, we calculated energetic properties using the gradient-corrected BP86[37,38] functional (GGA = generalized gradient approximation) in a self-consistent single-point fashion.[39] We calculated the binding energy E_b per thionyl ligand SCH_2CH_3 as the difference of total energies:

$$E_b = E_{tot}[SCH_2CH_3] + \{E_{tot}[Cu_{13}] - E_{tot}[Cu_{13}(SCH_2CH_3)_8]\}/8 \quad (5)$$

The energy of the ethylthionyl ligand was determined in the conformation it featured in the cluster. For instance, the energy of SCH_2CH_3 in the eclipsed configuration was taken as reference for a copper cluster with eclipsed ligands (see below).

For five isomers (buis, buie, tuis, tuie, buos; see below for definitions), we probed the basis set superposition error (BSSE). We compared results for the ligand shell $(SCH_2CH_3)_8$ (with eight unpaired electrons) obtained without and with accounting for the Cu_{13} basis set. Correspondingly, we compared results for Cu_{13} without and with accounting for the basis set of the ligand shell. The total energy of Cu_{13} was lowered by up to 11 kcal/mol due to the ligand basis set, and the ligand shell gained up to 4.5 kcal/mol due to the Cu_{13} basis set. As our discussion later on is based on relative values of E_{tot}, namely, differences to that energy for configuration buos (see below), we estimate the BSSE of these relative energies to, at most, 4.3 kcal/mol (E_b will be affected by, at most, 0.5 kcal/mol), based on the differences between the BSSE results for the isomers just mentioned and the result for isomer buos.

To represent the Kohn−Sham orbitals, we applied the following basis sets: C (9s5p1d) → [5s4p1d],[40] S (12s9p2d) → [6s5p2d],[41] H (6s1p) → [4s1p],[40] and Cu (15s11p6d) → [6s4p3d].[42,43] All contractions were of generalized form, based on LDA atomic eigenvectors. The auxiliary basis set utilized in the LCGTO-FF-DF method to represent the electron charge density for treating the Hartree part of the electron−electron interaction was constructed by scaling s and p exponents of the orbital basis sets using a standard procedure.[32] On each atom, five p- and five d-type "polarization" exponents were added, chosen as geometric series with factors 2.5, starting with 0.1 and 0.2 au, respectively. For the numerical integration of the exchange-correlation contributions, a superposition of atom-centered spherical grids[44] was chosen, using angular grids which are locally accurate up to angular momentum $L = 19$.[45]

For the MM calculations, we used the same force field as that in our previous work[15] where parameters suitable for modeling copper thiolates have been proposed and evaluated. For the metal−metal interaction, only the van der Waals interaction was parametrized because these interactions cancel in the IMOMM scheme.[15] For the organic components, like the alkyl chains, MM3 FF[29] parameters describing stretching, bending, and torsion potentials were adopted. Geometries were relaxed until all components of the Cartesian gradients were smaller than 10^{-5} au and also the update step length dropped below that same value.

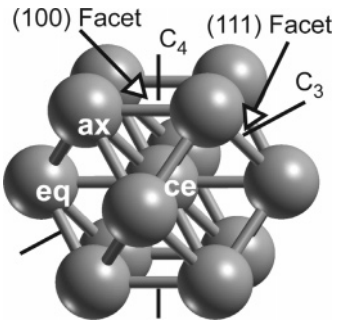

Figure 1. Cuboctahedral cluster Cu_{13} with labels of surface facets, pertinent C_n symmetry axes, and designators of the various atoms (ce = central, eq = equatorial, and ax = axial).

As expected, the QM/MM approach is computationally advantageous; for a given geometry, the time required for the electronic structure calculation (including the forces on the atoms) was reduced by about a factor of 2 compared to a QM calculation.

The Model Cluster $Cu_{13}(SCH_2CH_3)_8$

To examine the performance of the IMOMM approach for metal cluster compounds, we selected the copper thiolate cluster $Cu_{13}(SCH_2CH_3)_8$ in D_{4h} as a realistic but also computationally feasible model system. Ethylthionyl ligands are the shortest alkane thionyls for which steric interactions in the ligand shell are to be expected. In a recent study on $Au_{13}(SCH_3)_n$, we found that steric interactions are essentially absent between the smaller methylthionyl ligands.[46] For the Cu_{13} metal core, we adopted a cuboctahedral reference structure, comprising a central atom surrounded by a shell of 12 "surface" atoms. It is the smallest cluster that features a bulklike coordinated atom at its center. We preferred the cuboctahedral over the icosahedral shape of Cu_{13} because different ligand coordinations can easily be modeled. Also, the bare cluster Cu_{13} in I_h symmetry is 11 kcal/mol less stable; this result was not unexpected as the coinage metal cluster Au_{13} shows a similar preference.[39] During geometry optimization, we imposed D_{4h} symmetry constraints to restrict the structure of the ligand shell such that we were able to compare various ligand arrangements, optimized at both the DF and the QM/MM levels of theory. Overall, the cluster model chosen comprises all interactions present in larger transition metal thiolate clusters, yet it is simple enough to allow a full density functional treatment at the all-electron level for comparison.

Figure 1 introduces the designations of the various symmetry inequivalent Cu centers of the cluster. In D_{4h} symmetry, four surface atoms Cu_{eq} form a square in the horizontal (equatorial) symmetry plane, perpendicular to the C_4 main axis. Four metal atoms each form squares of (100) surface facets above and below that horizontal mirror plane; these centers Cu_{ax} are referred to as "axial". Finally, the central atom of the cluster is labeled as Cu_{ce}.

As reference, we optimized the bare metal core Cu_{13} both in O_h and D_{4h} symmetry. In O_h symmetry, all Cu−Cu bonds are equivalent and the LDA optimized bond length is 2.400

Å. The BP86 binding energy is 630 kcal/mol in total or 48.5 kcal/mol per atom. Because the highest occupied molecular orbital in O_h symmetry is only partially filled (t_{2g}^5), a Jahn−Teller distortion is expected, concomitant with a symmetry lowering. Applying D_{4h} symmetry constraints yielded two different isomers. The "round" isomer is bound with 631 kcal/mol and exhibits bonds that deviate, at most, 0.04 Å from those of the O_h reference. The other D_{4h} isomer features an overall oblate distortion where the equatorial atoms move outward ($Cu_{ce}-Cu_{eq} = 2.842$ Å) and the axial atoms move inward ($Cu_{ce}-Cu_{ax} = 2.296$ Å). With a BP86 atomization energy of 622 kcal/mol, this oblate structure is slightly less favorable than the O_h reference.

We adopted two starting configurations for the optimization of the ligated cluster $Cu_{13}(SCH_2CH_3)_8$. In the first case, ligands were singly coordinated to the axial Cu atoms—"on top" in the terminology of surface science. Alternatively, the ligands were attached to pairs of axial Cu atoms in 2-fold (bridge) coordination (Figures 2 and 3). We did not separately consider 3-fold coordination on the eight (111) facets of Cu_{13} because, in D_{4h} symmetry, ligands can move from bridging to (ideal) 3-fold positions. For the two starting configurations of D_{4h} symmetry, the S−C−C backbones of the ethylthionyl ligands lie in vertical mirror planes, limiting the number of possible conformations and, thus, facilitating a direct comparison of QM/MM and full QM results.

To distinguish different conformations of the ligands, we employ a labeling scheme that reflects the orientation of the ligands attached to the top facets of the cluster (Figures 2 and 3). First, the coordination of the ligands is classified as top (t) or bridging (b), according to the *starting* configuration; this designation is independent of where the ligands end up after optimization. For a ligand anchored on the metal cluster above the equatorial plane, the angle $Cu_{ax}-S-C$ (<180°) can be chosen to open upward (u) or downward (d) with respect to the C_4 main symmetry axis. In addition, the S−C−C moiety can be oriented toward (inward = i) or away from (outward = o) the C_4 axis. The last conformational degree of freedom in D_{4h} symmetry is the orientation of the terminal methyl group. It can be staggered (s) or eclipsed (e) with regard to the SCH_2 moiety. For example, the concatenated symbol "buos" designates a cluster isomer with bridging ligands (b), upward orientation (u) of the angle Cu−S−C, outward (o) opening of the angle S−C−C, and staggered conformation (s) of the methyl group. In summary, eight different conformers result for a given *initial* coordination mode (t or b), yielding a total of 16 conformers to be inspected.

According to experience with smaller compounds,[15] the C−C ligand bond has been chosen as the boundary between QM and MM regions. Thus, in the hybrid approach, the QM model was reduced to $Cu_{13}(SCH_3)_8$ and the terminal methyl groups of the ligands were treated at the MM level. The dangling C−C bonds were saturated by capping H atoms, using a constant ratio of the bond lengths, eq 4, with the scaling factor set to 0.709.[25] The boundary chosen between QM and MM partitions also accounts for the fact that charge transfer between these two regions is not included in the IMOMM model applied.

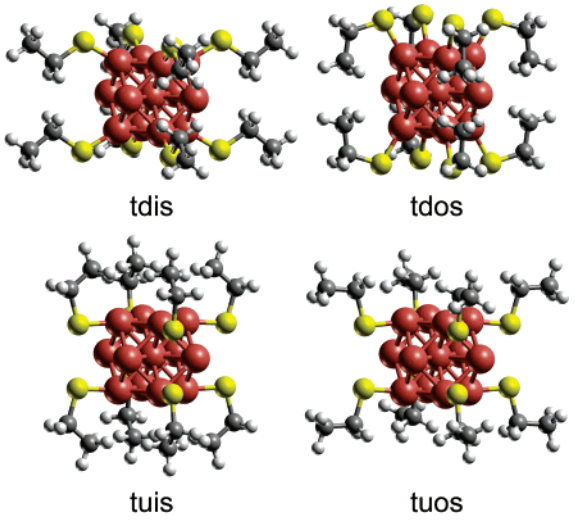

Figure 2. Four isomers of $Cu_{13}(SCH_2CH_3)_8$ with top coordination of the SCH_2CH_3 ligands and staggered orientation of the methyl group: ligands oriented downward−inward (tdis), downward−outward (tdos), upward−inward (tuis), and upward−outward (tuos).

QM Calculations on the Cluster $Cu_{13}(SCH_2CH_3)_8$

To set the stage for the evaluation of the QM/MM results on metal clusters, we first carried out QM reference calculations at the all-electron LDA level, optimizing structures for all 16 isomers. As visual inspection of optimized cluster geometries (Figures 2 and 3) reveals, ethylthionyl ligands are large enough so that steric effects play a role in the structure of the ligand shell of eight ligands assembled on the Cu_{13} cluster. Methyl end groups of top-coordinated ligands remain further from each other above the (100) facets because the ligands do not approach the cluster surface as closely as bridging ligands do. For the latter, this crowding effect is strongest for bdo isomers where the methyl end groups come close to each other near the horizontal symmetry plane (with shortest H−H contacts at 1.81 Å); there, methyl groups also get in close contact with Cu_{eq} atoms (with Cu−H = 1.97 Å). As top-coordinated ligands are further from the cluster surface, these contacts are weakened (shortest H−H at 2.18 Å and Cu−H at 2.43 Å) in tdo isomers (Figure 2).

For a detailed discussion of these observations, we have collected pertinent structure parameters in Table 1. We will first address "top" and then "bridge" isomers.

The cluster−ligand bond length $Cu_{ax}-S$ of top-coordinated ligands varies only slightly, between 2.10 and 2.13 Å, where the longer bonds are obtained for tdo isomers. Next-nearest copper−sulfur distances $Cu_{eq}-S$ exceed 3.7 Å for top ligands oriented downward, but they decrease to 3.1−3.2 Å for the upward orientation because ligands are shifted toward the equatorial plane (Figure 2). Ligand orientation also significantly affects the overall shape of the cluster as shown by the various Cu−Cu nearest-neighbor distances. The $Cu_{ce}-Cu_{eq}$ distance decreases along the series tui > tuo > tdi > tdo from ∼2.48 to 2.35 Å (Table 1). Concomitantly, the $Cu_{ce}-Cu_{ax}$ distance elongates, from ∼2.38 to ∼2.45 Å. Thus, the shape of the metal cluster core changes from oblate

Table 1. Characteristic Bond Lengths (in Å) of 16 Isomers of $Cu_{13}(SCH_2CH_3)_8$ Optimized with D_{4h} Symmetry Constraints[a]

isomer	$Cu_{ce}-Cu_{eq}$	$Cu_{ce}-Cu_{ax}$	$Cu_{eq}-S$	$Cu_{ax}-S$	$S-C_1$	C_1-C_2	$Cu_{ax}-S-C_1$
buis	2.339	2.662	2.298	2.193	1.853	1.500	118.4
buie	2.357	2.628	2.321	2.188	1.860	1.514	117.7
buos	2.345	2.604	2.365	2.201	1.860	1.503	115.4
buoe	2.356	2.614	2.326	2.196	1.863	1.516	119.4
bdis	2.283	2.573	2.837	2.236	1.847	1.510	109.5
bdie	2.286	2.572	2.835	2.234	1.850	1.523	109.8
bdos	2.299	2.603	3.281	2.254	1.815	1.493	113.6
bdoe	2.268	2.615	3.212	2.249	1.822	1.512	118.0
tuis	2.471	2.383	3.136	2.119	1.826	1.502	102.8
tuie	2.485	2.366	3.203	2.118	1.834	1.527	97.7
tuos	2.451	2.394	3.088	2.105	1.838	1.509	101.0
tuoe	2.449	2.400	3.077	2.103	1.835	1.525	104.8
tdis	2.402	2.409	3.708	2.101	1.823	1.510	116.3
tdie	2.403	2.408	3.707	2.101	1.824	1.522	116.6
tdos	2.345	2.459	4.113	2.134	1.817	1.501	104.0
tdoe	2.351	2.446	4.092	2.127	1.819	1.520	108.4
bdos[b]	2.859	2.500	2.173	2.244	1.850	1.503	138.6
bdoe[b]	2.868	2.500	2.168	2.239	1.859	1.512	138.7
tuis	2.471	2.383	3.136	2.119	1.826	1.502	102.8
tuie[b]	2.481	2.371	3.158	2.112	1.826	1.526	101.7

[a] For the designation of the various atoms, see Figure 1; for the designation of the isomers, see the text. [b] New isomers found with the help of IMOMM results.

to prolate. Clusters with "upward" oriented ligands exhibit longer distances from the center to the equatorial Cu atoms than in the corresponding conformation with the ligands oriented "downward". For instance, in td conformers, the $Cu_{ce}-Cu_{eq}$ bonds are ~0.1 Å longer than for the corresponding tu isomers (cf. tdi vs tui). Correspondingly, the $Cu_{ce}-Cu_{ax}$ distance is ~0.05 Å longer in td isomers than in the corresponding tu conformers.

The orientation of the methyl group, staggered or eclipsed, affects bond distances in a minor way, typically by 0.01 Å or less, but in some cases, these bonds can differ by up to ~0.02 Å between two corresponding isomers. Bond lengths within the ligands vary in similarly narrow ranges: 1.82−1.84 Å for $S-C_1$ and 1.50−1.53 Å for C_1-C_2. Bond angles for $Cu_{ax}-S-C_1$ are ~100° for tu, ~105° for tdo, and ~116° for tdi isomers.

The equilibrium geometries of clusters, where the structure optimization started with bridge-coordinated ligands, show rather different trends. An inspection of Figure 3 as well as a comparison of the distances $Cu_{ax}-S$ and $Cu_{eq}-S$ reveals that true 2-fold coordination is obtained only for the four types of isomers with downward-oriented ligands (bd). For these isomers, the $Cu_{ax}-S$ bond length is 2.23−2.25 Å, while the $Cu_{eq}-S$ distance remains considerably longer, ~2.8 Å for bdi isomers and ~3.2 Å for bdo structures (Table 1). Bridge-hollow coordination is found for the four types of bu isomers. There, the S atom lies still closer to the axial copper atoms, with $Cu_{ax}-S$ bonds of 2.19−2.20 Å, but the $Cu_{eq}-S$ contacts are only 0.11−0.17 Å longer, giving rise to some bonding interaction in these bridge-hollow coordination modes. In agreement with steric considerations, S atoms shift furthest to the 3-fold coordination site for bui rotamers (Figure 3). The ligands try to avoid the steric stress above the (100) facet by moving the S atom closer to the Cu_{eq} centers. $Cu_{ax}-S$ bonds of bridging ligands are systematically

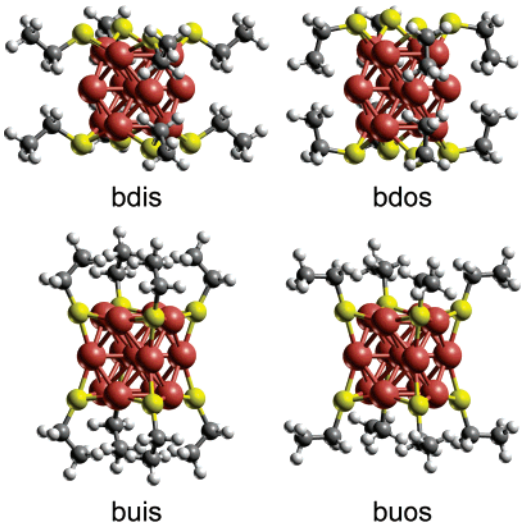

Figure 3. Four isomers of $Cu_{13}(SCH_2CH_3)_8$ with bridge coordination of the SCH_2CH_3 ligands and staggered orientation of the methyl group: ligands oriented downward−inward (bdis), downward−outward (bdos), upward−inward (buis), and upward−outward (buos).

longer than those of top-coordinated ligands by ~0.1 Å, as previously found for $Au_{13}(SMe)_n$ clusters.[46] A comparison of $Cu_{ce}-Cu_{eq}$ and $Cu_{ce}-Cu_{ax}$ bonds of a given isomer shows that all these structures are prolate, with the $Cu_{ce}-Cu_{ax}$ bonds longer by 0.26−0.35 Å; however, there is no clear trend as was found in the clusters with top-coordinated ligands. $Cu_{ce}-Cu_{eq}$ distances are 2.34−2.36 Å for bu isomers (with upward-oriented bridging ligands) and 2.27−2.30 Å for bd isomers (with downward-oriented ligands). The orientation of the methyl group affects Cu−Cu bonds in a similarly minor fashion as that in the top-coordinated clusters, with two exceptions: the two pairs buis−buie and bdos−bdoe feature changes of the $Cu_{ce}-Cu_{eq}$ and $Cu_{ce}-Cu_{ax}$ bonds, up

Table 2. Total Energies E_{tot} Relative to That of the Isomer buos and Binding Energies E_b Per Ligand for the Various Isomers of $Cu_{13}(SCH_2CH_3)_8$ as well as Corresponding Energy Differences ΔE_{tot} and ΔE_b between Staggered (s) and Eclipsed (e) Conformers of a Given Ligand Coordination Mode[a]

isomer	E_{tot}	ΔE_{tot}	E_b	ΔE_b
buis	1.7	−25.3	62.9	0.6
buie	26.9		62.3	
buos	0.0	−23.3	63.1	0.3
buoe	23.3		62.8	
bdis	30.1	−25.3	59.4	0.6
bdie	55.4		58.8	
bdos	64.7	−21.3	55.0	0.1
bdoe	86.0		55.0	
tuis	106.2	−40.4	49.8	2.5
tuie	146.6		47.4	
tuos	102.8	−25.3	50.3	0.6
tuoe	128.1		49.7	
tdis	122.7	−25.8	47.8	0.6
tdie	148.5		47.1	
tdos	151.1	−18.9	44.2	−0.2
tdoe	170.0		44.4	
bdos[b]	2.2	−23.5	62.8	0.3
bdoe[b]	25.7		62.5	
tuis	106.2	−31.3	49.8	1.3
tuie[b]	137.4		48.5	

[a] Energies in kcal/mol. [b] New isomers found with the help of IMOMM results.

to 0.03 Å, in opposite directions. The bond lengths within the ligands also vary within similar margins as those for cluster isomers with top coordination: 1.82−1.86 Å for $S-C_1$ and 1.49−1.52 Å for C_1-C_2. $Cu_{ax}-S-C_1$ angles are 114−120° for bu as well as bdo isomers and are 110° for bdi isomers.

Comparing clusters of the same ligand orientation, one finds $Cu_{ce}-Cu_{eq}$ bonds for top coordination longer than for bridge coordination and $Cu_{ce}-Cu_{ax}$ bonds shorter. $Cu_{ce}-Cu_{eq}$ bonds can differ by 0.08−0.13 Å, and $Cu_{ce}-Cu_{ax}$ bonds can differ by 0.14−0.28 Å (Table 1).

In Table 2, we compare various energetic parameters of the 16 isomers. The total energy is referenced to that of the most stable isomer, buos. In general, isomers with bridging ligands are 90−120 kcal/mol more stable than isomers with top-coordinated ligands of the same orientation. While the total energies of isomers with bridging ligands span an interval of ∼85 kcal/mol, the energies of isomers with top-coordinated ligands scatter over an interval of ∼70 kcal/mol. The most stable isomer with top-coordinated ligands, tuos, is 17 kcal/mol less stable than the least stable isomer with bridge-coordinated ligands, bdoe, and more than 100 kcal/mol less stable than the most stable isomer, buos. These energy differences result from variations of the ligand binding energies E_b, which are 11−15 kcal/mol for a given ligand orientation (Table 2).

Among the "top" conformers, tdo isomers exhibit the smallest ligand binding energies, ∼44 kcal/mol, followed by tdi isomers with ∼47 kcal/mol; tu isomers have the largest ligand binding energies, ∼50 kcal/mol. The binding energy of bridge-coordinated ligands varies typically between 55 and 63 kcal/mol and shows the same ordering as that for top-coordinated ligands. bdo isomers have the lowest binding energy, 55 kcal/mol, followed by bdi isomers with 59 kcal/mol and bu isomers with ∼63 kcal/mol. Because E_b values are referenced to corresponding rotamer structures, staggered and eclipsed, they show more clearly than E_{tot} values the direct ligand−cluster interaction including steric effects. This conclusion is supported by the very small differences ΔE_b between corresponding values of staggered and eclipsed structures (Table 2).

As expected, the eclipsed form of the ethyl end group leads to a higher total energy. For isolated ethylthionyl ligands SCH_2CH_3, the energy difference between staggered and eclipsed conformations was calculated at 2.6 kcal/mol. The corresponding rotational barrier of ethylthiol $HSCH_2CH_3$ is calculated slightly higher, at 3 kcal/mol. For a cluster with eight ligands, these values extrapolate to ∼21 and 24 kcal/mol, respectively. Accordingly, the energies of most pairs of rotamers between staggered (s) and eclipsed (e) conformations differ by 23−25 kcal/mol (see ΔE_{tot}, Table 2). For the bdo and tdo isomers, this energy difference ΔE_{tot} is ∼3 and 5 kcal/mol, respectively, smaller (by absolute value) than the average value of 24 kcal/mol; however, these energy variation values translate into binding energy changes of less than 1 kcal/mol per ligand (see ΔE_b, Table 2). Only the tui rotamers are separated notably further in energy as the eclipsed rotamer is 40 kcal/mol less stable than the corresponding staggered structure. This increase of the energy difference is due to specific ligand−ligand interactions which are enforced by the constraints of the ligand conformation (Figure 2). Indeed, in the tuie conformation, the energy of the ligand shell $(SCH_2CH_3)_8$ (in a configuration with eight unpaired spins) is 13.6 kcal/mol *destabilized* relative to the energy of eight isolated ligands in the eclipsed conformation. Yet, a single ethylthionyl in the optimized conformation of the tuie isomer is only 0.1 kcal/mol less stable than the free ligand. In contrast, the ligand shell $(SCH_2CH_3)_8$ is *stabilized* by 5.1 kcal/mol relative to the energy of eight isolated ligands in a staggered conformation. Thus, the unusual high destabilization of the eclipsed tui rotamer derives from an unfavorable interligand interaction.

As expected, we determined a doublet ground state for all but two isomers of the cluster $Cu_{13}(SCH_2CH_3)_8$, reflecting the odd number of electrons of the system. The tdo pair of isomers was found to be more stable in the quartet state. For structures with bridging ligands, the gap between highest occupied and lowest unoccupied spin−orbitals is 0.5−0.9 eV, whereas it is considerably smaller, 0.05−0.2 eV, for isomers with terminal ligand coordination, rationalizing to some extent the exceptional quartet state of two t-type structures.

Finally, we mention additional cluster isomers of the td type with an overall oblate shape (not listed in the tables), which we found when we tried to use the flat, bare Cu_{13} as an underlying cluster core. Because these cluster conformations represent states of higher energy compared to their prolate congeners (E_{tot} 3.7 kcal/mol higher for tdie and tdoe,

Table 3. Characteristic Geometric Parameters of the Cu_{13} Cluster Core and the Cluster−Ligand Interface of 16 Conformers of $Cu_{13}(SCH_2CH_3)_8$ from QM/MM Calculations and Deviations δ(QM/MM-QM) from the Corresponding QM Results[a]

isomer	$Cu_{ce}-Cu_{eq}$	δ	$Cu_{ce}-Cu_{ax}$	δ	$Cu_{eq}-S$	δ	$Cu_{ax}-S$	δ	$Cu_{ax}-S-C_1$	δ
buis	2.368	0.029	2.644	−0.018	2.287	−0.011	2.187	−0.006	124.1	5.6
buie	2.370	0.013	2.631	0.003	2.314	−0.006	2.188	0.000	121.9	4.2
buos	2.357	0.012	2.619	0.015	2.322	−0.043	2.193	−0.008	118.4	3.1
buoe	2.358	0.003	2.620	0.006	2.320	−0.006	2.192	−0.004	118.4	−1.0
bdis	2.276	−0.007	2.578	0.005	2.874	0.036	2.234	−0.002	107.2	−2.3
bdie	2.276	−0.009	2.579	0.006	2.882	0.047	2.234	−0.001	107.0	−2.9
bdos	2.807	0.508	2.509	−0.095	2.177	−1.104	2.240	−0.014	138.8	25.2
bdoe	2.811	0.543	2.507	−0.108	2.177	−1.035	2.235	−0.014	138.3	20.2
tuis	2.485	0.014	2.368	−0.015	3.163	0.027	2.111	−0.007	113.1	10.2
tuie	2.483	−0.002	2.369	0.003	3.169	−0.034	2.109	−0.008	116.7	18.9
tuos	2.482	0.030	2.376	−0.018	3.132	0.044	2.112	0.006	102.9	1.9
tuoe	2.482	0.033	2.376	−0.024	3.132	0.055	2.111	0.008	103.0	−1.9
tdis	2.394	−0.007	2.414	0.005	3.733	0.025	2.103	0.003	113.0	−3.3
tdie	2.395	−0.008	2.414	0.005	3.735	0.027	2.103	0.002	112.9	−3.8
tdos	2.349	0.005	2.442	−0.017	4.072	−0.041	2.116	−0.018	116.1	12.1
tdoe	2.339	−0.011	2.445	−0.001	4.069	−0.023	2.115	−0.013	121.8	13.3
bdos[b]	2.807	−0.053	2.509	0.009	2.177	0.005	2.240	−0.004	138.8	0.2
bdoe[b]	2.811	−0.057	2.507	0.007	2.177	0.008	2.235	−0.004	138.3	−0.4
tuis	2.485	0.014	2.368	−0.015	3.163	0.027	2.111	−0.007	113.1	10.2
tuie[b]	2.483	0.002	2.369	−0.002	3.169	0.011	2.109	−0.003	116.7	14.9

[a] Bond lengths and their differences in Å; angles and their differences in degrees. [b] Differences to new DF isomers found with the help of IMOMM results.

5.5 kcal/mol for tdis, and 7.4 kcal/mol for tdos), we will not discuss them further.

IMOMM Calculations on the Cluster $Cu_{13}(SCH_2CH_3)_8$

To assess the applicability and accuracy of the IMOMM QM/MM approach for metal cluster compounds, we will now compare IMOMM results to those obtained previously in all-electron QM calculations. At first, we used the very same initial structures for the QM/MM geometry optimizations as those used previously for the pure QM optimizations—to locate, as far as possible, the same local minima. We will begin with discussing the results of these optimizations. For some isomers, this strategy failed to identify analogous local minima, and we had to expand our search, as will be detailed later on.

To characterize the consequences of the different computational methods, we will start with a discussion of the largest structural deviations. The geometric parameters of IMOMM-optimized cluster compounds are displayed in Table 3, together with the deviations from the corresponding QM results. An inspection of the bond distances and their deviations reveals that the largest differences between QM and QM/MM results occur for the bdo isomers; below, we will discuss these structures separately. For the remaining structures, the average absolute deviations are 0.013 Å (0.033 Å) for $Cu_{ce}-Cu_{eq}$, 0.010 Å (0.024 Å) for $Cu_{ce}-Cu_{ax}$, 0.030 Å (0.055 Å) for $Cu_{eq}-S$, 0.006 Å (0.018 Å) for $Cu_{ax}-S$, and 6.0° (18.9°) for $Cu_{ax}-S-C_1$; the maximum absolute deviations are given in parentheses. From these values, one concludes that the IMOMM method works rather well for such ligated metal cluster compounds. Distances $Cu_{ax}-S$ are particularly well-reproduced. In contrast, discrepancies in the angles $Cu_{ax}-S-C_1$ indicate a propensity for easy deformation in this structural characteristic. As these angles are not stabilized by any additional direct bond, they react strongly on (small) changes in the environment and, therefore, can be used as sensitive indicators for (other) very small structural discrepancies. According to this criterion, the isomers bdo, tui, and tdo deserve special attention (Table 3) as the discrepancies in the angles range from 10 to 25°. Also, the bui isomers, with differences in the $Cu_{ax}-S-C_1$ angle of 4−6°, can be mentioned in this context.

We first turn to the bdo isomers, which show the largest structural differences between IMOMM and full QM calculations. In the QM/MM structures, the $Cu_{eq}-S$ distances are significantly elongated, more than 1 Å, compared to the corresponding QM structures (Table 3). This strong discrepancy reflects the displacement of the ligands from bridge sites in the QM-optimized structure to 3-fold hollow positions in the QM/MM case (Figure 4). Also, the structures of the Cu_{13} core differ noticeably between the two types of calculations. In the IMOMM calculations, the $Cu_{ce}-Cu_{eq}$ distances are ∼0.5 Å longer and the axial bonds $Cu_{ce}-Cu_{ax}$ are 0.1 Å shorter. Thus, the shape of the cluster core as determined by the QM/MM calculations is quite similar to that of the oblate bare cluster Cu_{13}. Recall that the latter isomer of the bare cluster is only ∼10 kcal/mol less stable than the prolate isomer. These very substantial differences for the bdo isomers between the results of the two computational methods, which obviously do not present the same minimum at the potential energy surface, can be traced to the corresponding ligand arrangements. In the all-electron case, the ligands of the bdo rotamers wrap around the cluster surface (Figure 4), resulting in rather short contacts (<2.5 Å) between the methyl groups of the ligands and the Cu_{eq} centers. In the bdoe conformer, the corresponding $Cu_{eq}-H$ contacts are just 1.97 Å, but this distance is 2.31 Å in the bdos isomer. One expects this

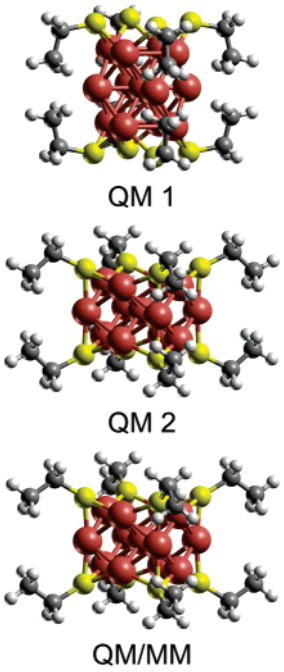

Figure 4. Geometries of the bdos isomer with bridge-coordinated ligands in "downward" orientation with outward-pointing methyl tail groups. Structures from full DF (QM1) and QM/MM calculations which have been started from the same initial structure as well as the DF (QM2) result which has been obtained when starting from the QM/MM geometry.

nonbonding interaction to be clearly repulsive. Indeed, the QM/MM structure (Figure 4) seems to imply a strong repulsion as the $Cu_{eq}-H$ contacts elongate substantially, to 3.29 Å in the bdoe conformer and to 3.57 Å in the bdos conformer.

These significant differences between the results for the bdo structures can be attributed to the different representation of nonbonding interactions by the DF and FF methods. The currently popular exchange-correlation approximations of LDA and GGA types are unable to account for dispersion interaction in a quantitative fashion,[47] although some success has recently been claimed with specially parametrized functionals as well as a time-dependent density-functional theory approach.[48−52] For the LDA functional applied here, this methodological deficiency becomes manifest in too-short nonbonding contacts[53] which may be rationalized by an artificial attraction due to density overlap;[54] this failure is also observed for GGA functionals.[54] In addition, a common feature of all mathematically local density functionals is the missing dispersion interaction.[47,54] On the other hand, force fields explicitly account for van der Waals interaction via their parametrization. Thus, for short nonbonding contacts, one can expect proper repulsion and, consequently, more reliable results from a FF (or a QM/MM) approach than from a pure DFT-based method. Furthermore, if nonbonding contacts are present, the risk of locating different minima in QM/MM and DF optimizations is increased as a result of artificial stabilization of nonbonding contacts in LDA or GGA calculations.[54]

As a check of this hypothesis, we evaluated the difference ΔE_{MM} of the force-field energy contributions at QM- and QM/MM-optimized geometries for the isomers bdo, buo, tui, and tdo:

$$\Delta E_{MM} = [E_{MM}(XY) - E_{MM}(X)]_{QM\ geometry} - [E_{MM}(XY) - E_{MM}(X)]_{QM/MM\ geometry} \quad (6)$$

We chose the isomers with the largest deviations between QM and QM/MM and one pair with small structure differences as counterexamples (buo). More than 95% of ΔE_{MM} derives from van der Waals interaction. Just as expected, ΔE_{MM} values for the bdo isomers are unusually large, more than 400 kcal/mol. Also, the ΔE_{MM} of isomer tuie is quite large, 330 kcal/mol. The analogous values for other conformers are notably smaller, 109 kcal/mol for tdoe, 52 kcal/mol for tdos, and 60 kcal/mol for tuis. As expected, ΔE_{MM} values are very small, 1.1 and 6.6 kcal/mol, for the buo counterexamples.

According to these findings, QM and QM/MM results for other isomers with short interligand H−H or Cu−H contacts should also differ. Indeed, bui, tui, and tdo conformers (in addition to the bdo structures) exhibit such relatively short interligand contacts. Cu−H contacts of the tdo isomers from the all-electron QM calculations (with Cu_{ax}: tdos − 2.77 Å and tdoe − 2.43 Å) are quite a bit longer than in the bdo isomers (2.31 and 1.97 Å; see above). Consequently, differences between QM and QM/MM results for bond lengths were considerably smaller for tdo than for bdo isomers, although $Cu_{ax}-S-C$ bond angles increased notably in the tdo isomers, by 12−13° (Table 3). In the same spirit, relatively short H−H contacts of about 2.3 and 2.5 Å for the tuis and tuie isomers, respectively, did not prevent good agreement among bond distances obtained from QM and QM/MM calculations but were reflected in larger values of $Cu_{ax}-S-C$ angles from QM/MM calculations, 10° (tuis) and 19° (tuie). For bui isomers, the structural trends seem comparable to those of the tui isomers, but the changes in the $Cu_{ax}-S-C$ angles are much smaller (Cu−H = 3.11 and 3.16 Å and H−H = 2.42 and 1.91 Å for buie and buis, respectively). Because bridge-coordinated ligands are closer to the "surface" of the cluster core, they have to bend less to form H−H contacts comparable to those of tui structures. For the tuie isomer, even a very short $Cu_{ax}-H$ contact of 2.085 Å was obtained in the full QM calculation.

The structures with close Cu−H and H−H contacts are the very same structures that we previously had singled out with the help of the criterion of the $Cu_{ax}-S-C_1$ angles. Whereas the $Cu_{ax}-S-C_1$ angles from QM/MM and full QM calculations differ noticeably in the bui, tdo, and tui conformers, bond distances deviate, at most, by 0.04 Å. Apparently, the ligands are just differently oriented, but the individual structures of both the ligands and the cluster core remain largely unchanged. Indeed, the shape of the clusters stays oblate for "bridge" coordination and prolate for "top" coordination. Also, the IMOMM approach yields the same 2- or 3-fold coordination as that of the full QM calculations.

The differences between the results from the QM and QM/MM approaches are reflected by the energetics as well (Table 4). Also, for the IMOMM calculations, we use the buos structure as an energy reference. Bridge-coordinated

Table 4. Relative Total Energies E_{tot}, Binding Energies E_b Per Ligand from QM/MM Calculations on 16 Conformers of $Cu_{13}(SCH_2CH_3)_8$, and Corresponding Energy Differences ΔE_{tot} and ΔE_b between Staggered (s) and Eclipsed (e) Conformers of a Given Ligand Coordination Mode. Also Shown Are the Differences δE_{tot} and δE_b from the Corresponding QM Energies[a]

isomer	E_{tot}	ΔE_{tot}	δE_{tot}	E_b	ΔE_b	δE_b
buis	−6.9	−30.9	8.6	66.7	−0.2	−3.8
buie	24.0		2.9	67.0		−4.6
buos	0.0	−34.1	0.0	65.8	0.2	−2.7
buoe	34.1		−10.9	65.7		−2.9
bdis	32.7	−34.7	−2.7	61.7	0.2	−2.4
bdie	67.4		−12.1	61.5		−2.7
bdos	−3.0	−39.7	67.7	66.2	0.8	−11.2
bdoe	36.6		49.3	65.4		−10.4
tuis	100.2	−45.8	6.0	53.3	1.6	−3.5
tuie	146.0		0.6	51.7		−4.3
tuos	100.7	−34.8	2.1	53.2	0.2	−3.0
tuoe	135.5		−7.4	53.0		−3.3
tdis	126.2	−34.6	−3.6	50.1	0.2	−2.3
tdie	160.8		−12.3	49.8		−2.7
tdos	127.8	−43.0	23.3	49.9	1.3	−5.6
tdoe	170.8		−0.8	48.6		−4.2
bdos[b]	−3.0	−39.7	5.2	66.2	0.8	−3.4
bdoe[b]	36.6		−10.9	65.4		−2.9
tuis	100.2	−45.8	6.0	53.3	1.6	−3.5
tuie[b]	146.0		−8.6	51.7		−3.2

[a] Energies in kcal/mol. [b] Differences to new DF isomers found with the help of IMOMM results.

clusters have IMOMM energies that are up to 68 kcal/mol higher than that of the reference, spanning an interval of 74 kcal/mol, compared to 86 kcal/mol at the full QM level. The relative total energies of top-coordinated clusters fall into the range from 100 to 171 kcal/mol, compared to 103−170 kcal/mol at the full QM level. The energy separation of clusters with bridge- and top-coordinated ligand shells is somewhat more pronounced at the QM/MM level (33 kcal/mol) than at the full QM level (16 kcal/mol).

The buos structure features a low energy also at the IMOMM level, but the buis and bdos structures are somewhat lower in energy. At the QM/MM level, the buis structure is 8.6 kcal/mol stabilized compared to the full QM calculation (δE_{tot}, Table 4). In fact, the total energies from both types of calculations correlate reasonably well (Figure 5), with differences δE_{tot} typically ranging from −12 to 9 kcal/mol, with three rather notable exceptions: the structures bdos (68 kcal/mol), bdoe (49 kcal/mol), and tdos (23 kcal/mol). Below, we will discuss these structures in more detail.

As in the full QM calculations, isomers with staggered methyl substituents are always more stable than those with an eclipsed orientation of the methyl groups. The differences ΔE_{tot} from the IMOMM calculations, ranging now from 31 to 46 kcal/mol, are notably larger than those from the full QM calculations. IMOMM values typically are close to 34 kcal/mol, 10 kcal/mol larger than typical QM values (Table 4). This difference is traced back to corresponding differences for the isolated thionyl ligands: In the QM/MM approach, the rotational barrier of the ethyl end group is calculated at 4.0 kcal/mol, whereas a full DF treatment yields a value of 2.6 kcal/mol. Test calculations on ethane yielded rotational barriers of 2.9 kcal/mol for QM/MM and 2.6 kcal/mol for QM, in good agreement with experimental values (2.9 kcal mol[55]).

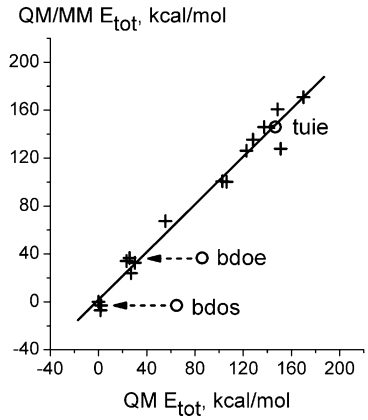

Figure 5. Correlation of E_{tot}, QM vs QM/MM values (in kcal/mol). Crosses denote results of corresponding minima; circles refer to deviating minima obtained when invoking the same starting condition in the optimization. For details, see text.

The ligand binding energies E_b from full QM calculations are very well reproduced with the IMOMM approach. Ligand binding energies of bridge-coordinated structures from IMOMM calculations, 62−67 kcal/mol, are again notably larger than those of top-coordinated structures, 49−53 kcal/mol. These E_b values show the same independence of the orientation of the methyl substituents (staggered vs eclipsed) when referenced to the appropriate rotamer structure; the largest difference ΔE_b is 1.6 kcal/mol. An inspection of Table 4 reveals that the ligand binding energies E_b from the IMOMM calculations are consistently larger than those from full QM calculations, by 2.3−5.6 kcal/mol if one leaves aside the bdo isomers with δE_b values of −11.2 and −10.4 kcal/mol, respectively. These differences are mainly due to approximating ethylthionyl ligands by their methylthionyl congeners in the QM subsystem of the IMOMM calculations.[15] Slight variations among the (regular) ligand binding energies, for example, from $\delta E_b = -2.7$ kcal/mol for buos to $\delta E_b = -3.8$ kcal/mol for buis, stabilize the latter structure and cause it to become the ground state of the QM/MM calculations.

We did not observe major differences in the electronic structure between QM and QM/MM results, although the QM system in the IMOMM approach is reduced to $Cu_{13}(SCH_3)_8$. As in the QM calculations, doublet ground states were obtained for all isomers except for the pair tdo, for which, again, quartet states were determined. Gaps between highest occupied and lowest unoccupied spin−orbitals amounted to 0.6−0.85 eV for structures with bridge-coordinated ligands and to 0.05−0.1 eV for structures with terminally coordinated ligands, again, in good agreement with the QM results. Thus, truncation of the ligand at the first CC bond also preserves essential features of the electronic structure of the cluster in the QM/MM calculation.

After this examination of the QM/MM results and their deviations from a full DF treatment, we note adequate overall similarity between the energetics at the two levels of theory. The bdo isomers with their artificially close Cu−H contacts at the all-electron DF level have already been identified as special cases when we analyzed the structures. Above, we had concluded that IMOMM structures are more realistic than the pure QM structures, which are significantly higher in energy for bdo isomers (by 50−70 kcal/mol; Table 4). Given these large energy differences, it seems worth studying whether the more realistic energetics at the QM/MM level in fact produce a local minimum that corresponds to the one located previously at the all-electron QM level.

To probe this conjecture, we started all-electron QM structure optimizations from *all* geometries optimized at the IMMOM level. Indeed, for 3 of the 16 isomers, we found new minima with lower full QM total energies than obtained previously. It is not too surprising that the two special structures bdos and bdoe were among them; the new QM structures turned out to be substantially more stable (by 62.5 and 60.3 kcal/mol, respectively) than the old QM structures. The third case was the isomer tuie, also discussed before as a case with unusually close nonbonding contacts (see above); its new QM structure is, by 9.2 kcal/mol, more stable. As expected, ΔE_{MM} values characterizing the van der Waals repulsion decreased substantially for the new QM structures (bdos: 11 kcal/mol; bdoe: 40 kcal/mol; tuie: 177 kcal/mol). The corresponding structure and energy data for the bdo and tui isomers are displayed in the lower sections of Tables 1−4. Note that there is only one QM structure for the tuis isomer; the corresponding data are shown to allow a full comparison of all table entries.

The new bdo structures are now the only bridge-coordinated systems for which we found an oblate cluster core (Figure 4, QM2). Their ligands are 3-fold bound, as in the bu isomers. The S−C bond lengths of the new structures now fit better with values for other clusters with bridging ligands. The new, full QM structures of the bdo isomers agree well with the corresponding QM/MM structures, with the largest differences (0.053−0.057 Å) occurring for the $Cu_{ce}-Cu_{ax}$ distances (Table 3). The new QM structure of the tuie isomer is structurally quite similar to the old one, also yielding a relatively large difference of 14.9° to the QM/MM result of the sensitive angle $Cu_{ax}-S-C_1$ (Table 3). Now, the average absolute (and maximum) deviations between the QM and QM/MM results of *all* isomers are 0.018 Å (0.057 Å) for $Cu_{ce}-Cu_{eq}$, 0.010 Å (0.024 Å) for $Cu_{ce}-Cu_{ax}$, 0.026 Å (0.055 Å) for $Cu_{eq}-S$, 0.006 Å (0.018 Å) for $Cu_{ax}-S$, and 5.1° (14.9°) for $Cu_{ax}-S-C_1$.

The three new isomers also fit the energetic characteristics of their congeners very well. The energy difference ΔE_{tot} between the staggered and eclipsed tui conformers is now reduced to −31.3 kcal/mol from, previously, −40.4 kcal/mol (Table 2). Most noticeable is the agreement of the new QM energies for the bdo isomers with the corresponding QM/MM values; the δE_{tot} values (bdos: 5.2 kcal/mol; bdoe: −10.9 kcal/mol) now fall in the normal range (see above and Table 4). With these new total energies, the correlation between QM and QM/MM improves drastically; the regression coefficient r^2 for the values of E_{tot} increases from 0.87 for the original data to, now, 0.98 (Figure 5). A similar improvement is observed for the differences δE_b between QM and QM/MM ligand binding energies. The deviation, previously ∼10 kcal/mol, decreased to less than 4 kcal/mol (bdos: −3.4 kcal/mol; bdoe: −2.9 kcal/mol; Table 4).

From this reoptimization of QM structures, we conclude that the overestimation of nonbonding interactions in the DF approach may lead to local minima that are different from those obtained with the IMOMM approach because the DF energetics favor structures involving artificially close contacts. Of course, on a potential energy surface in a high-dimensional space, it is quite difficult with a standard optimization procedure to avoid localizing a metastable local minimum instead of the true ground state. Yet, it is encouraging that, in the example discussed above, the more realistic treatment of van der Waals interactions in the QM/MM approach resulted in the identification of low-lying minima.

Conclusions

We carried out the first QM/MM study on a ligand-protected d metal cluster, using a density-functional-based IMOMM approach. As a model compound, we chose the copper thiolate cluster $Cu_{13}(SCH_2CH_3)_8$, imposing D_{4h} symmetry constraints to enable the evaluation of ligand arrangements with bridge-hollow and top coordination at the Cu_{13} cluster core. We considered various orientations of the ligands relative to the surface of the metal particle as well as staggered and eclipsed forms of the ethyl end group of the ligands, yielding a test set of 16 conformers. Structures have been optimized with an LDA functional; energies were evaluated in single-point fashion using a GGA functional. To assess the performance and accuracy of the IMOMM approach, we optimized all 16 isomers of $Cu_{13}(SCH_2CH_3)_8$ at both the all-electron DF and the QM/MM levels, using one starting geometry for each isomer.

With some exceptions, we found that the QM/MM approach reproduces the results of the full QM calculations in satisfactory fashion, for both structure and energy data. The structures of a pair of staggered and eclipsed rotamers (bdoe/bdos) showed close Cu−H or H−H contacts in the (original) QM structures which were not reproduced in the corresponding QM/MM calculations. In that case, QM and QM/MM results for structure and energetics differed substantially. Less severe differences were found for other isomers exhibiting short nonbonding contacts (buis/buie, tuis/tuie, and tdos/tdoe). In the DF calculations with standard exchange-correlation functionals, such close nonbonding contacts lead to artificial attractive interactions which are absent in QM/MM calculations when van der Waals interactions are handled at the MM level. Reoptimization of all QM structures starting from QM/MM-optimized geometries yielded new QM structures for those three isomers that previously had exhibited the strongest deviations from QM/MM results. The isomers of bdo obtained with the new, full QM calculations exhibit ∼0.8 Å longer Cu−H distances (bdoe 2.76 Å, bdos 3.24 Å). Nevertheless, the H−H contacts increased by only 0.2 Å for bdoe compared to the old isomer. Figure 4 (QM2) reveals that even the ligands approach each

other more closely in the new, full DF structures than in those obtained with the QM/MM treatment. Thus, one obtains overall good agreement between QM and QM/MM calculations. The shortcomings regarding nonbonding interactions displayed by the DF approach, based on a standard exchange-correlation functional, in general, lead to small deviations of structural and energetic results. For certain cases with the largest structural discrepancies, the optimization actually had resulted in two different local minima.

On the basis of this study, we conclude that the IMOMM approach is capable of treating metal cluster compounds comprising extended ligand shells. However, one has to be aware of potential deviations from a full quantum mechanical treatment when short nonbonding contacts occur, especially across the boundary of the QM and MM parts of the model. This issue is particularly crucial if the QM treatment is based on LDA or GGA density functional calculations. Such exchange-correlation functionals are known to fail for nonbonding (dispersion) interactions. Thus, in contrast to other systems, one may expect that a QM/MM approach, employing a suitably parametrized force field, will yield more reliable results for systems involving many van der Waals contacts in the ligand shell or across the boundary of the QM and MM regions.

Acknowledgment. This work was supported by Deutsche Forschungsgemeinschaft, Volkswagen Foundation, and Fond der Chemischen Industrie.

References

(1) Thiel, W. *THEOCHEM* **1997**, *398*−*399*, 1.

(2) Monard, G.; Merz, K. M., Jr. *Acc. Chem. Res.* **1999**, *32*, 904.

(3) Sherwood, P.; de Vries, A. H.; Guest, M. F.; Schreckenbach, G.; Catlow, C. R. A.; French, S. A.; Sokol, A. A.; Bromley, S. T.; Thiel, W.; Turner, A. J.; Billeter, S.; Terstegen, F.; Thiel, S.; Kendrick, J.; Rogers, S. C.; Casci, J.; Watson, M.; King, F.; Karlsen, E.; Sjøvoll, M.; Fahmi, A.; Schäfer, A.; Lennartz, C. *THEOCHEM* **2003**, *632*, 1.

(4) Maseras, F.; Morokuma, K. *J. Comput. Chem.* **1995**, *16*, 1170.

(5) Woo, T. K.; Pioda, G.; Röthlisberger, U.; Togni, A. *Organometallics* **2000**, *19*, 2144.

(6) Woo, T. K.; Margl, P. M.; Deng, L.; Cavallo, L.; Ziegler, T. *Catal. Today* **1999**, *50*, 479.

(7) Lopez, N.; Pacchioni, G.; Maseras, F.; Illas, F. *Chem. Phys. Lett.* **1998**, *294*, 611.

(8) Fischer, D.; Curioni, A.; Andreoni, W. *Langmuir* **2003**, *19*, 3567.

(9) Kerdcharoen, T.; Liedl, K. R.; Rode, B. M. *Chem. Phys.* **1996**, *211*, 313.

(10) Bryce, R. A.; Vincent, M. A.; Hillier, I. H. *J. Phys. Chem. A* **1999**, *103*, 4094.

(11) Kerdcharoen, T.; Morokuma, K. *Chem. Phys. Lett.* **2002**, *355*, 257.

(12) Ryde, U. *J. Comput.-Aided Mol. Des.* **1996**, *10*, 153.

(13) Eichinger, E.; Tavan, P.; Hutter, J.; Parrinello, M. *J. Chem. Phys.* **1999**, *110*, 10452.

(14) Eurenius, K. P.; Chateld, D. C.; Brooks, B. R. *Int. J. Quantum Chem.* **1996**, *60*, 1189.

(15) Kerdcharoen, T.; Birkenheuer, U.; Krüger, S.; Woiterski, A.; Rösch, N. *Theor. Chem. Acc.* **2003**, *109*, 285.

(16) Andres, R. P.; Bielefeld, J. D.; Henderson, J. I.; Janes, D. B.; Kolagunta, V. R.; Kubiak, C. P.; Mahoney, W. J.; Osifchin, R. G. *Science* **1996**, *273*, 1690.

(17) Daniel, M.-C.; Astruc, D. *Chem Rev.* **2004**, *104*, 293.

(18) Chen, S.; Sommers, J. M. *J. Phys. Chem. B* **2001**, *105*, 8816.

(19) Ang, T. P.; Wee, T. S. A.; Chin, W. S. *J. Phys. Chem. B* **2004**, *108*, 11001.

(20) Tempelton, A. C.; Wuelfing, W. P.; Murray, R. W. *Acc. Chem. Res.* **2000**, *33*, 27.

(21) Hostetler, M. J.; Wingate, J. E.; Zhong, C.-Z.; Harris, J. E.; Vachet, R. W.; Clark, M. R.; Londono, J. D.; Green, S. J.; Stockes, J. J.; Wignall, G. D.; Glish, G. L.; Porter, M. D.; Evans, N. D.; Murray, R. W. *Langmuir* **1998**, *14*, 17.

(22) Belling, T.; Grauschopf, T.; Krüger, S.; Mayer, M.; Nörtemann, F.; Staufer, M.; Zenger, C.; Rösch, N. In *High Performance Scientific and Engineering Computing; Lecture Notes in Computational Science and Engineering*; Bungartz, H.-J., Durst, F., Zenger, C., Eds.; Springer: Berlin, 1999; Vol. 8, p 439.

(23) Belling, T.; Grauschopf, T.; Krüger, S.; Nörtemann, F.; Staufer, M.; Mayer, M.; Nasluzov, V. A.; Birkenheuer, U.; Hu, A.; Matveev, A. V.; Shor, A. M.; Fuchs-Rohr, M.; Neyman, K.; Ganyushin, D. I.; Kerdcharoen, T.; Woiterski, A.; Gordienko, A.; Majumder, S.; Rösch, N. *ParaGauss*, version 3.0; Technische Universität München: Munich, Germany, 2004.

(24) Singh, U. C.; Kollman, P. A. *J. Comput. Chem.* **1986**, *7*, 718.

(25) Dapprich, S.; Komaromi, I.; Byun, K. S.; Morokuma, K.; Frisch, M. J. *THEOCHEM* **1999**, *461*, 1.

(26) Shor, A.; Rösch, N. Unpublished results.

(27) Nörtemann, F. Dissertation, Technische Universität München, Munich, Germany, 1998.

(28) Matveev, A. V.; Mayer, M. M.; Rösch, N. *Comput. Phys. Commun.* **2004**, *160*, 91.

(29) Allinger, N. L.; Yuh, Y. H.; Lii, J.-H. *J. Am. Chem. Soc.* **1989**, *111*, 8551.

(30) Hayes, D. M.; Barber, M.; Clark, J. H. R. *J. Chem. Soc., Faraday Trans. 2* **1977**, *73*, 1485.

(31) Perram, J. W.; Petersen, H. G.; De Leeuw, S. V. *Mol. Phys.* **1988**, *65*, 875.

(32) Dunlap, B. I.; Rösch, N. *Adv. Quantum Chem.* **1990**, *21*, 317.

(33) Vosko, S. H.; Wilk, L.; Nusair, N. *Can. J. Phys.* **1980**, *58*, 1200.

(34) Ziegler, T. *Chem. Rev.* **1991**, *91*, 651.

(35) Krüger, S.; Seemüller, T.; Wörndle, A.; Rösch, N. *Int. J. Quantum Chem.* **2000**, *80*, 576.

(36) Desmarias, N.; Jamorski, C.; Reuse, F. A.; Khanna, S, N. *Chem. Phys. Lett.* **1998**, *294*, 480.

(37) Becke, A. D. *Phys. Rev. A* **1988**, *38*, 3098.

(38) Perdew, J. P.; Wang, Y. *Phys. Rev. B* **1986**, *33*, 8800.

(39) Häberlen, O. D.; Chung, S.-C.; Stener, M.; Rösch, N. *J. Chem. Phys.* **1997**, *106*, 5189.

(40) van Duijnefeldt, F. B. *IBM Res. Rep.* **1971**, RJ945.

(41) Veillard, A. *Theor. Chim. Acta* **1968**, *12*, 405.

(42) Wachters, A. J. H. *J. Chem. Phys.* **1970**, *52*, 1033.

(43) Hay, P. *J. Chem. Phys.* **1977**, *66*, 4377.

(44) Becke, A. D. *J. Chem. Phys.* **1988**, *88*, 2547.

(45) Lebedev, V. I. *Zh. Vychisl. Mat. Mat. Fiz.* **1976**, *16*, 293.

(46) Genest, A.; Krüger, S.; Gordienko, A. B.; Rösch, N. *Z. Naturforsch., B: Chem. Sci.* **2004**, *59b*, 1585.

(47) Holthausen, M. C.; Koch, W. *A Chemist's Guide to Density Functional Theory*; Wiley-VCH: Weinheim, Germany, 2000.

(48) Osinga, V. P.; van Gisbergen, S. J. A.; Snijders, J. G.; Baerends, E. J. *J. Chem. Phys.* **1997**, *106*, 5091.

(49) Wu, Q.; Yang, W. *J. Chem. Phys* **2002**, *116*, 515.

(50) Langreth, D. C.; Dion, M.; Rydberg, H.; Schröder, E.; Hyldgaard, P.; Lundqvist, B. I. *Int. J. Quantum Chem.* **2005**, *101*, 599.

(51) Goddard, W. A., III. Private communication.

(52) Furche, F.; van Voorhis, T. *J. Chem. Phys.* **2005**, *122*, 164106.

(53) Pérez-Jordá, J. M.; Becke, A. D. *Chem. Phys. Lett.* **1995**, *233*, 134.

(54) van Mourik, T.; Gdanitz, R. J. *J. Chem. Phys.* **2002**, *116*, 9620.

(55) Wilson, E. B. *Adv. Chem. Phys.* **1959**, *2*, 367.

CT050202R